Minimal model for aeolian sand dunes

Klaus Kroy
Department of Physics and Astronomy, University of Edinburgh, Edinburgh EH9 3JZ, United Kingdom

Gerd Sauermann and Hans J. Herrmann
ICA-1, Universität Stuttgart, Pfaffenwaldring 27, 70569 Stuttgart, Germany
(Received 11 March 2002; published 13 September 2002)

We present a minimal model for the formation and migration of aeolian sand dunes in unidirectional winds. It combines a perturbative description of the turbulent wind velocity field above the dune with a continuum saltation model that allows for saturation transients in the sand flux. The latter are shown to provide a characteristic length scale, called saturation length, which is distinct from the saltation length of the grains. The model admits two different classes of solutions for the steady-state profile along the wind direction: smooth heaps and dunes with slip face. We clarify the origin of the characteristic properties of these solutions and analyze their scaling behavior. We also investigate in some detail the dynamic evolution of heaps and dunes, including the steady-state migration velocity and transient shape relaxation. Although the minimal model employs nonlocal expressions for the wind shear stress as well as for the sand flux, it is simple enough to serve as a very efficient tool for analytical and numerical investigations and opens up the way to simulations of large scale desert topographies.

DOI: 10.1103/PhysRevE.66.031302 PACS number(s): 45.70.Mg, 45.70.Qj, 47.27.−i, 51.10.+y

I. INTRODUCTION

The study of sand dunes has a long and colorful history [1–3], but a sound understanding of the physical mechanisms behind dune formation and migration has proved elusive, let alone the accurate prediction of the evolution of whole desert topographies. Simple questions such as the following seemed theoretically very difficult to answer: What determines the shape of dunes? How fast do they move? Is there a minimum or maximum dune size? Though sand dunes develop wherever sand is exposed to an agitating medium that can lift grains from the ground, they cannot easily be scaled down to be studied in the lab. With the macroscopic phenomena of interest separated by many orders of magnitude from the grain scale and involving various coupled nonlinear processes such as turbulent air flow and grain hopping (''saltation''), one is bound to devise some simplified models in order to address such questions. We will argue that approximate numerical models can only be successful if based on a sound qualitative understanding of the problem. Therefore, our main aim is to identify the key mechanisms underlying dune formation and migration and incorporate them into a working minimal model of aeolian sand dunes, and we will emphasize generic aspects over the more specific details. For definiteness, the reader may find it helpful to think of isolated transverse dunes or crescent-shaped barchan dunes as major applications of the model. The broad phenomenology of aeolian (and submarine) land forms provides a large number of different characteristic sand structures that can certainly not all be described by the same simple model developed with the specific examples of barchan or transverse dunes in mind. However, we expect that our approach is amenable to future adaptations that make it applicable to a broader class of sand topographies on the one hand, and for quantitative investigations of more specific questions on the other hand. Although the minimal model refers only to rather generic properties of the wind velocity field and the laws of aeolian sand transport, it can make interesting predictions about the surface profile, the development and position of the slip face, dune migration, etc., which are insensitive to the simplifying assumptions. The main features of the model have already been briefly presented in a recent letter [4]. The present contribution gives a more comprehensive discussion of the model and tries to communicate its precise definition as well as its major predictions to an interdisciplinary readership. The model, as presented here, is restricted to a two-dimensional (2D) slice of a dune parallel to the unidirectional wind. (A generalization to 3D problems is in preparation.) A further restriction is the neglect of ripples and direct slope effects onto the sand transport outside slip faces. Although they have successfully been incorporated into continuum sand transport models [5–7] similar to our own [8], we chose to disregard them for the present purpose and leave their integration to future work.

The paper is organized as follows. In the following introductory section we summarize some background knowledge and basic definitions. We will also introduce a naive ''zeroth-order'' description of the wind shear stress and the induced aeolian sediment transport. Its instructive failure to produce dunelike steady-state solutions will be a guide for identifying two relatively small effects (the upwind shift of the maximum of the shear stress with respect to the topography and the saturation transients in the sand flux) as key ingredients of a proper description of structure formation by aeolian sand transport. We will, moreover, derive the scaling behavior of the migration velocity for translation invariant heaps and dunes of different sizes but similar shapes based on very general grounds. Sections III and IV are devoted to the definition of the minimal model, i.e., to the modeling of the air shear stress exerted onto a heap of sand and the induced sand transport, respectively. The first step builds on turbulent

boundary layer calculations developed in a series of publications mainly by Hunt and co-workers [9–14], the second one on a previous contribution [8] by the present authors. Only the most pertinent results of these earlier developments will be summarized here. In the remainder, we will derive some important predictions of the model for the central slice of a barchan dune or transverse dune. In particular, we will demonstrate that there is a minimal dune size. Although we will thereby gain interesting results, these are rather meant to be illustrative examples of possible applications of the model. By no means do we attempt to provide a complete analysis of its predictions, and it should become obvious that much more remains still to be done. Finally we will summarize our main results and speculate about probable consequences of the present 2D theory for 3D topographies.

II. GENERAL

A. Aeolian sand transport

Before going into the description of the model, we want to recall some general background and introduce some quantities of major interest. First of all, for convenience, we will usually refer to dunes without slip face as heaps. Further, we will sometimes find it helpful to focus on isolated heaps or dunes on bedrock, although most of our discussion is not restricted to this situation.

The key quantity for the description of the formation and migration of sand dunes and heaps is the local horizontal surface velocity $v(x,t)$ of a sand height profile $h(x,t)$ at all positions x and times t. Via mass conservation it can be related to the erosion rate $\nabla q(x,t)$ (negative erosion is deposition), where the sand flux $q(x,t)$ is defined as the mass of sand transported per unit of time across a hyperplane transverse to the wind direction. More precisely, since we want to specialize our discussion to a 2D slice parallel to the unidirectional wind velocity, the hyperplane is a vertical line and q is actually a mass transport rate per unit width. Mass conservation then takes the form of a continuity equation for the height profile,

$$\varrho_s \frac{dh(x,t)}{dt} = -\frac{\partial q(x,t)}{\partial x}, \tag{1}$$

with ϱ_s being the density of the sand bed.

With Eq. (1) one can write the position dependent migration velocity at a given time t as

$$v(x) = \varrho_s^{-1} \frac{q'}{h'}, \tag{2}$$

where we have introduced the shorthand notation $f'(x) \equiv df(x)/dx$. At this stage we can already get some physical insight by observing that this equation needs special attention at the top of a heap or dune, where we expect the denominator to vanish. For v to remain finite at the crest as required in the steady state, there are in general only two possibilities. Either the sand flux q is fine tuned so that the erosion q' vanishes in exactly the same way as the slope h', or the profile $h(x)$ is not differentiable at the crest. As the reader may already anticipate and will be verified below, both cases have their physical realizations, the former in heaps or small dunes with smooth crests and the latter in large dunes with a slip face that terminates in a sharp brink at the crest.

The problem we face, if we want to calculate the dynamic evolution of desert topographies, is the closure of Eq. (1) or Eq. (2) by expressing the flux $q(x,t)$ in terms of the height profile $h(x,t)$ and the external wind and boundary conditions. Since for the applications we have in mind, the migration velocity is very small compared to the speed of elementary sand transport processes (grain hopping, etc.) and the wind speed, the topography can be assumed to be stationary for considerations concerning the wind and sand transport dynamics. This allows one to subdivide the problem of calculating $q(x)$ into two independent steps. First, one needs to know the stationary wind velocity above a given topography. More precisely, what is required is the shear stress τ exerted by the wind onto the ground. And second, one needs a model that predicts the stationary sand flux $q(x)$ for a given stationary $\tau(x)$, schematically

$$h(x) \rightarrow \tau(x), \tag{3}$$

$$\tau(x) \rightarrow q(x). \tag{4}$$

Computing the derivative q' and integrating the mass conservation equation (1) then closes the model and allows one to predict the development of the surface profile in time. Since aeolian dunes typically have relatively gentle slopes outside their slip face, we restrict the scope of the minimal model to this case at the present stage, and have disregarded in Eq. (4) (outside of slip faces) the direct slope effects $h'(x) \rightarrow q(x)$ onto the flux.

In special cases, the relations (3) and (4) are phenomenologically and theoretically well established. For a flat surface, $h(x) \equiv$ const, it is well known [15] that the mean turbulent wind velocity increases logarithmically with height above the surface. It can be characterized by a single characteristic velocity, the shear velocity u_* defined by $u_*^2 \equiv \tau_0/\varrho_a$ with τ_0 the (suitably time averaged) shear stress and ϱ_a the density of air. The shear stress of the air is transmitted to the surface as a friction that can mobilize grains on a surface covered with sand if it exceeds a threshold value τ_t. As a result, the wind entrains some grains into a surface layer flow. The grains advance mainly by an irregular hopping process (saltation), thereby reducing the wind velocity in the surface layer. Via this feedback mechanism a unique relation between the shear stress τ and the sand flux q is established in the equilibrium state. If τ is not too close to the threshold, this relation can approximately be represented as [1]

$$q_s \propto \tau^{3/2}. \tag{5}$$

Although a host of more accurate descriptions have been discussed in the literature [2,8,16–18] and one of them will be part of our definition of the minimal model below, the simpler Eq. (5) will be sufficient for our qualitative discussion in the first part of the paper. The index s in Eq. (5)

emphasizes that such local relations are restricted to situations where the flux is saturated, that is, equal to the equilibrium transport capacity. This is certainly not the case near a boundary between uncovered and covered ground or on sloped beds. Neglecting this restriction for the moment, Eq. (5) predicts that the shear stress perturbation

$$\hat{\tau}(x) \equiv \tau(x)/\tau_0 - 1 \tag{6}$$

above a modulated topography $h(x)$ is responsible for flux gradients dq_s/dx that cause erosion and deposition and thus—according to Eqs. (1) and (2)—migration of the sand surface. Explicitly closing the model by assuming that the shear stress is an affine function of the modulation of the topography ($\hat{\tau} \propto h$) leads to what we call the zeroth-order model, which will briefly be analyzed in the following section paragraph.

B. Failure of the zeroth-order model

The zeroth-order model is given by

$$\hat{\tau}\{h(x)\} \to \hat{\tau}(h) \propto h(x)/L, \tag{7}$$

$$q\{\tau(x)\} \to q(\tau) = q_s(\tau), \tag{8}$$

where we have used the curly brackets to indicate a general functional dependence and introduced a characteristic length scale L of the topography to normalize the height profile. (The motivation for the latter step will become clear in the following section.) The zeroth-order model assumes *local* relations in Eqs. (3) and (4). It approximates the wind shear stress perturbation by its ''affine'' contribution (proportional to the profile h that causes the perturbation) and replaces the true sand flux q by its saturated value q_s, thereby neglecting saturation transients. This model is so simple that its qualitative predictions for an arbitrary smooth heap of sand can easily be anticipated without any actual calculations.

Combining Eq. (2) with Eqs. (5)–(8) one obtains a surface velocity that increases with height ($dv/dh \geqslant 0$) due to the nonlinearity of Eq. (5). This implies that the upwind (or ''stoss'') slope tends to decrease and the downwind (or ''lee'') slope tends to increase. Since $dq/dx \propto dh/dx$ by the chain rule, there is no erosion or deposition at the top of a smooth heap, which therefore keeps its initial height. Obviously, integrating forward in time will eventually increase the lee slope up to the angle of repose, where surface avalanches have to be introduced and a slip face of constant slope develops. If the latter reaches the crest, the above argument for the persistence of the height can no longer be applied, because the slope at the crest is then ill defined. Since there is so far nothing to stop a further decrease of the windward slope, the model dune will then start to decrease in height and finally flatten out. The steady-state solution is a flat surface.

The simple argument shows that the zeroth-order model—although it gives some clue as to the origin of the slip face—is insufficient for a proper qualitative understanding of dunes. However, some important lessons can be learned from it that will be helpful in our further investigation of the problem. First, even with a very simplistic model any reasonably heaplike initial condition will quickly develop into a dunelike shape with a slip face. Second, although the latter may seem to converge to a steady-state solution for intermediate times, it finally turns out to be unstable and flattens out. The discussion of the migration velocity in Sec. II A suggests that small deviations from Eqs. (7) and (8) at the brink can make an important difference. Obviously some caution is needed in judging the success of numerical models of dune formation. Unless stability has explicitly been demonstrated, they may be suspected to fail in a similar way as the zeroth-order model when integrated over sufficiently long times (which has actually not been checked for some models that can be found in the literature) or to be sensitive to numerical errors at the brink. Detailed numerical modeling should therefore be preceded by a sound qualitative understanding of the mechanisms underlying dune formation. We will argue in Secs. III and IV that to this end a subtle balance between two small deviations from Eqs. (7) and (8) and especially nonlocal contributions in Eq. (4) have to be taken into account.

C. Migration velocity

Before entering a detailed discussion of the minimal model, it is worth pausing for some general thoughts as to what can be said about the shear stress and the speedup of the wind above an obstacle, without actually doing the (somewhat involved) calculation.

A basic property of strongly developed turbulence is its dilation invariance or scale-free structure. Whereas general Navier-Stokes flow is invariant under a scale transformation that keeps the Reynolds number constant, strongly turbulent flow (for ''infinite'' Reynolds number) allows for infinitely many such similarity transformations. Landau and Lifshitz [15] took advantage of this fact for deriving the logarithmic velocity profile mentioned above by an elegant scaling argument. The logarithmic velocity profile suggests that the speedup of the wind and therefore also the shear stress perturbation above a heap of given shape should itself be logarithmically dependent on its size. But how do they depend on the shape of the obstacle? Since the flow itself does not provide any characteristic length scale, the dimensionless quantity $\hat{\tau}$ defined in Eq. (6) can only depend on a dimensionless characterization of the profile $h(x)$. In other words, to lowest order in the perturbation, it must be a linear functional of the derivative h' and can be written as

$$\hat{\tau}(\xi) = \varepsilon\, \mathcal{T}\{f'(\xi)\}, \quad \varepsilon \equiv H/L, \tag{9}$$

with a dimensionless profile function

$$f(\xi) \equiv h(x)/H, \quad \xi \equiv x/L \tag{10}$$

and a scale-free (and necessarily nonlocal) linear functional $\mathcal{T}$. This reasoning can be repeated for the dimensionless velocity and pressure perturbations. Intuitively, the scaling $\hat{\tau} \propto \varepsilon$ for a flat smooth obstacle ($\varepsilon \ll 1$) can be understood from Fig. 1. When the air flows over the obstacle, the velocity close to the obstacle is deflected by an angle ε whereas it remains constant far above the obstacle. For incompressible

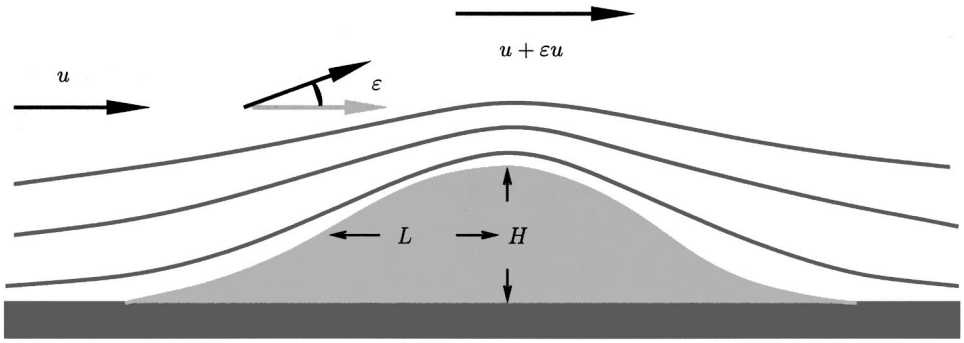

FIG. 1. Schematic sketch of the deflection of the wind velocity u above a flat heap of aspect ratio $\varepsilon \equiv H/L \ll 1$. The characteristic length scale L is in this context conventionally often identified with the half length at half height of the heap. The vertical deflection causes a speedup above the top of the heap. This is accompanied by a pressure perturbation that is negative above the top of the heap and positive at its tails. Due to turbulence, the flow pattern is asymmetric even above a symmetric heap.

flow, continuity translates this into a speedup of order ε and (via Bernoulli's law) into a corresponding pressure drop near the top of the heap. This in turn causes a shear stress perturbation $\hat{\tau}$ of the same order.

These general considerations already allow us to predict the scaling of the migration velocity v with dune size if we assume that dunes of different size have roughly similar shapes $f(\xi)$ and aspect ratios ε, which is indeed suggested by the scale invariance of the turbulent wind field and by observations. Inserting Eq. (9) into Eq. (2), and again approximating Eq. (4) by a local sand transport law $q \equiv q(\tau)$, we find

$$v \frac{dq}{d\hat{\tau}} \frac{d\hat{\tau}/dx}{\varrho_s \varepsilon f'} = \frac{dq}{d\hat{\tau}} \frac{\mathcal{T}\{f'\}}{\varrho_s L f'} \propto \frac{1}{L}. \tag{11}$$

The final proportionality strictly holds only if the steady-state shape $f(\xi)$ and aspect ratio ε are scale invariant. However, it can be expected to be robust and rather insensitive against violations of exact scale invariance. First, the normalized steady-state shapes $f(\xi)$ are strongly constrained by the requirement that they render $v(x) \equiv v$, independent of x, along the heap. Therefore, they should to a first approximation be independent of size, which is indeed borne out by the minimal model (Fig. 13) and empirical observations [19]. Moreover, the dependence $v\{f'(\xi)\}$ is rather indirect and can therefore be expected to be weak. Second, Eq. (5) suggests that for gently sloped obstacles ($\varepsilon \ll 1$) the dependence of $dq/d\tau$ on the aspect ratio ε also is not very pronounced. And finally—due to the above mentioned scale invariance of turbulence—a scale invariant aspect ratio can reasonably be expected for large dunes. In fact, we will show below that the minimal model predicts that the aspect ratio of small heaps is not constant but rather decreases proportional to their height. But this also implies that the latter becomes too small to have a very significant effect on the above argument. Note, however, that only for strictly scale invariant dunes, Eq. (11) becomes identical to the often quoted observation that dunes migrate with a speed inversely proportional to their height [20]. Since the deviations of large dunes from scale invariance are not very pronounced, the difference between these predictions is only noticeable for small dunes and heaps. Presently available field data are maybe not accurate enough to clearly distinguish between $v \propto 1/L$ and $v \propto 1/H$, though some data support $v \propto 1/L$, most notably the comprehensive study of barchan dunes in southern Peru by Finkel [21]. As we will show below, our numerical results for the minimal model clearly favor $v \propto 1/L$.

We also note that together with Eq. (5), Eq. (11), moreover, predicts that the migration velocity grows nonlinearly with (as the third power of) the wind velocity. A more accurate relation can be obtained from the minimal model as described below, but the qualitative conclusion is the same. Dunes can migrate farther in a short period of exceptionally strong wind than during much longer periods of gentle winds. Finally, we should mention that some caution is needed when identifying the characteristic length scale L in Eq. (11). In our discussion, we have so far assumed that $f(\xi)$ is a smooth function, which is not the case for dunes with slip face. Below we will argue that in this case f should be identified with the envelope of the dune and its separation bubble and L with the characteristic length scale of this envelope. For a barchan dune the latter practically coincides with the total length of the dune from its windward end to the tips of its horns.

In contrast to the overall migration velocity of a translation invariant dune, the position dependent migration velocity $v(x)$ that determines the shape is much harder to obtain since it requires a precise knowledge of the nonlocal functional $\mathcal{T}$ in Eq. (9). This will be provided in the following section.

III. WIND SHEAR STRESS

A. Surface shear stress on a smooth heap

The discussion in the preceding section showed that—in contrast to the assumption in Eq. (7)—the dependence of the shear stress on the height profile is nonlocal. Although it will turn out that this shortcoming of Eq. (7) is not responsible for the failure of the zeroth-order model, it should by now have become apparent that further progress can hardly be achieved without a rather detailed understanding of the turbulent wind field above heaps and dunes. For dunes with a slip face that typically has a slope of about 32°–35° and

terminates in a sharp brink, the situation is similar to the textbook example of a backward facing step, which has the reputation of a test case for numerical turbulent models. Even if a commercial turbulent solver is used, the accurate calculation of the shear stress, e.g., on a barchan dune is a nontrivial task and quite demanding in computer time and memory, and the most interesting long-time dynamics of dunes is therefore difficult to access. For this reason, we want to focus on flat smooth heaps first. In this case, one can apply an analytical perturbation theory for turbulent boundary layer flow over smooth hills that has been developed over the last decades [9–14]. Though the calculation is essentially a formalization of the intuitive description accompanying Fig. 1, it requires a highly nontrivial boundary layer construction that we will not recapitulate here. The interested reader is referred to the original literature. We merely quote the final result for the x component (along the main wind direction) $\hat{\tau}_x$ of the surface shear stress perturbation above a profile $h(x,y)$ [12,14],

$$\mathcal{F}_{xy}\{\hat{\tau}_x\}=\frac{Ak_x(k_x+iB|k_x|)}{(k_x^2+k_y^2)^{1/2}}\mathcal{F}_{xy}\{h(x,y)\}. \tag{12}$$

We have abbreviated the Fourier transformation from the space variables x, y to the respective wave numbers k_x, k_y by $\mathcal{F}_{xy}$. For simplicity the logarithmic k dependence of the parameters A and B was neglected. The latter are then given by

$$A=\frac{\ln(\Phi^2/\ln\Phi)^2}{2(\ln\phi)^3}[1+\ln\phi+2\ln(\pi/2)+4\gamma],$$

$$B=\pi/[1+\ln\phi+2\ln(\pi/2)+4\gamma_E], \tag{13}$$

$$\phi\equiv 2\kappa^2\Phi/\ln\phi,$$

and depend logarithmically on the ratio $\Phi\equiv L/z_0$, where L is the characteristic length of $h(x,0)$ (for this purpose, conventionally often identified with half the length at half height or about one-fourth of the characteristic wavelength) and z_0 is a measure of the surface roughness (typically an effective length somewhat below the linear dimension of the latter). We also have introduced the von Kármán constant $\kappa\approx 0.4$ and Euler's constant $\gamma_E\approx 0.577$. A practical approximation for ϕ is obtained by iterating (twice) the implicit equation for ϕ and closing it by dropping the remaining $\ln\phi$. The dependence of A and B on L is depicted in Fig. 2. Obviously, as long as L/z_0 does not change by orders of magnitude (e.g., due to vegetation), this extremely weak scale dependence is negligible for our purposes, and A and B can be regarded as constant theoretical or phenomenological parameters. For definiteness we often work with the values $A=4$ and $B=0.25$ (approximately obtained for $L/z_0=10^5$–10^6). Although these values may vary somewhat depending on the particular application in mind, or on the presence or absence of ripples, and may phenomenologically be somewhat different from the theoretical prediction, this does not affect our general conclusions.

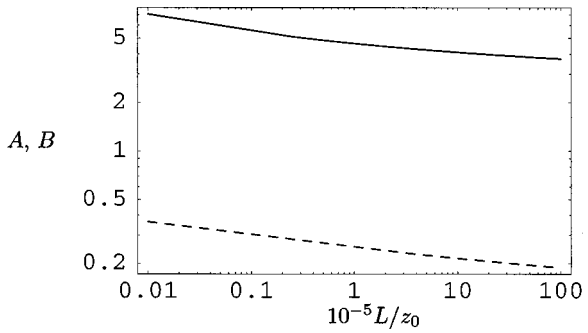

FIG. 2. The theoretical prediction for the dependence of the parameters A (solid line) and B (dashed line) of Eq. (13) on the ratio of the dune size L to the roughness length z_0.

For the following discussion we want to specialize Eq. (12) to the central slice of a transverse or barchan dune along the wind direction. To this end we evaluate Eq. (12) for the central slice $h(x)$ of a heap that has a Gaussian shape with standard deviation σ in the transverse direction parametrized by y,

$$h(x,y)=h(x)e^{-y^2/2\sigma^2}. \tag{14}$$

This approximation is technically useful, and although it may seem relatively crude for a particular real dune, it typically does not introduce any noteworthy derogation of the results compared to a more accurate description. The Fourier coefficients of the shear stress $\hat{\tau}(x)\equiv\hat{\tau}_x(x,0)$ on the central slice along the wind direction become

$$\mathcal{F}\{\hat{\tau}(x)\}=\frac{\sigma A}{\sqrt{2\pi}}k(k+iB|k|)\times e^{-1/4k^2\sigma^2}K_0\left(\frac{k^2\sigma^2}{4}\right)\mathcal{F}\{h(x)\}. \tag{15}$$

Here, K_0 denotes a modified Bessel function and the Fourier transforms are one dimensional, so that we can drop the redundant x subscripts.

For transverse dunes ($\sigma/L\to\infty$), we obtain the two equivalent expressions

$$\mathcal{F}\{\hat{\tau}^\infty(x)\}=A(|k|+iB\,k)\mathcal{F}\{h(x)\}, \tag{16a}$$

$$\hat{\tau}^\infty(x)=A[h'(x)\otimes(\pi x)^{-1}+Bh'(x)]. \tag{16b}$$

For the real space version we have abbreviated a convolution integral according to

$$f\otimes g\equiv\int_{-\infty}^{\infty}d\xi\, f(\xi)g(x-\xi). \tag{17}$$

Evaluation for arbitrary σ gives two correction terms

$$\hat{\tau}^\sigma=\hat{\tau}^\infty-A(h\otimes\Delta_1+Bh'\otimes\Delta_2), \tag{18}$$

with

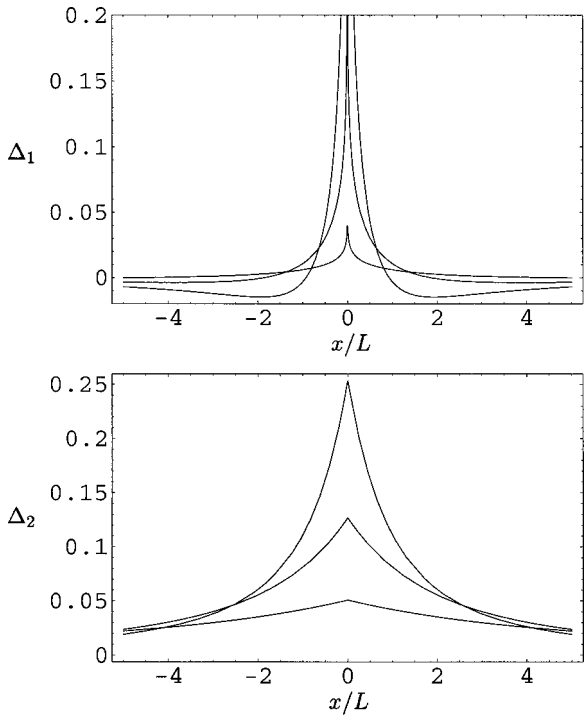

FIG. 3. The peaked functions Δ_1 and Δ_2 of Eqs. (19) and (20) for $\sigma=1$, 2, 5. The area under the peaks remains constant (0 and $1/2\pi$), while the peak heights decrease proportional to σ^{-2} and σ^{-1}, respectively.

$$\Delta_1=\frac{U\left(\frac{3}{2},1,\frac{x^2}{2\sigma^2}\right)}{4\sqrt{\pi}\sigma^2}+\frac{\sqrt{\pi}}{2}\frac{U\left(\frac{1}{2},0,\frac{x^2}{2\sigma^2}\right)-1}{\pi x^2}, \tag{19}$$

$$\Delta_2=\frac{1}{\sigma\pi}\int_0^\infty d\xi\cos\left(\frac{\xi x}{\sigma}\right)\left[1-\frac{\xi e^{\xi^2/4}}{\sqrt{2\pi}}K_0\left(\frac{\xi^2}{4}\right)\right], \tag{20}$$

two even functions depicted in Fig. 3 that are flat for $\sigma/L\to\infty$ and become peaked for $\sigma\simeq L$. (The confluent hypergeometric U functions [22] have been introduced to rephrase the sine part of the Fourier integrals.)

Since the correction terms in Eq. (18) are numerically small, we may—given a reasonable localized heap shape in the wind direction—approximately replace both functions Δ_1 and Δ_2 by δ functions, thus arriving at

$$\hat{\tau}_\sigma\approx\hat{\tau}_\infty-A[c_1(\sigma)h+Bc_2(\sigma)h']. \tag{21}$$

In this approximation they are seen to give merely a σ-dependent renormalization of the asymmetry parameter $B\to B(\sigma)\lesssim B(\infty)=B$ and to add a (trivial) term $c_1(\sigma)h(x)$ within the brackets of Eq. (16b). Numerically, one can estimate $L\,c_1(L/\sqrt{2})$ and $c_2(L/\sqrt{2})$ to be about 0.2 (cf. Fig. 4). The exact σ dependence of the coefficients is determined by the shape and extension of the heap in the x direction, because the area under the peaks Δ_1 and Δ_2 is constant and independent of σ, while the peak height decreases proportional to σ^{-2} and σ^{-1}, respectively. Since both corrections vanish for $\sigma/L\to\infty$ and do not contribute any substantial

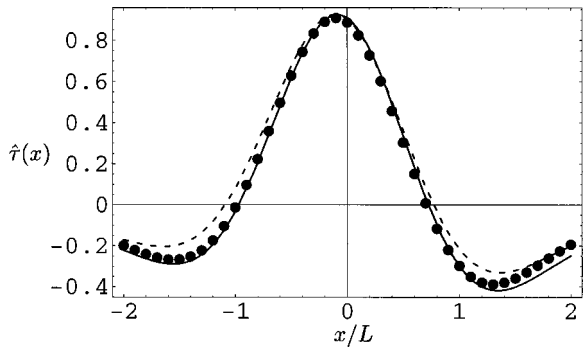

FIG. 4. Shear stress perturbation above the central slice of a 3D symmetric ($\sigma=L/\sqrt{2}$) Gaussian heap. The plot compares two approximations to Eqs. (12) and (18) (points): (i) Eq. (21) with $Lc_1\approx c_2\approx 0.2$ (solid line) and (ii) Eq. (16) with A renormalized by a factor 0.8 (dashed line). While (i) is practically indistinguishable from Eq. (12) on the present level of accuracy, the simpler approximation (ii) already captures most of the 3D effects.

new effects to Eq. (16), they may for simplicity be omitted altogether in the following discussion that mainly aims at a qualitative understanding. Figure 4, moreover, shows that they can approximately be mimicked by a renormalized parameter A in Eq. (16) for the central slice of a symmetric heap. This leads to the important conclusion that the wind shear stress on the central slice of a 3D symmetric heap and on a heap with a profile that is constant in the transverse direction is qualitatively the same and quantitatively similar, which was not *a priori* obvious. Together with the fact that on a gently sloped obstacle the transverse components of the shear stress are small compared to its longitudinal components, this suggests that the predictions of Eq. (16) apply in a first approximation to any slice of a dune parallel to the wind direction. In this sense, the study of Eq. (16) is representative. Summarizing the foregoing discussion, we can say that to gain a qualitative understanding of dune formation by aeolian sand transport one may focus on Eq. (16) as a model for the wind shear stress. We therefore analyze this equation in some detail in the following section.

B. Properties and consequences of Eq. (16)

A scaling analysis of Eq. (16) immediately reveals that $\hat{\tau}$ is indeed of the general form anticipated on general grounds in Eq. (9). The amplification of the shear stress at the top of a smooth profile is thus determined by its aspect ratio $\varepsilon=H/L$ and is essentially independent of the absolute height H. It only has a very weak logarithmic dependence on the absolute size of the dune through the prefactors A and B given in Eq. (13). Moreover, for a symmetric profile $f(-\xi)=f(\xi)$, $\hat{\tau}$ is the sum of a symmetric part and an antisymmetric part, i.e., the flow over the heap has a symmetry breaking component that is a consequence of turbulence. The origin of the symmetric and antisymmetric parts of $\hat{\tau}$ can intuitively be understood as follows. As we have pointed out in Sec. II C (see Fig. 1), the streamlines have to be compressed above the heap if the perturbation is not to be transmitted to infinite height, and as a consequence, there is a

corresponding increase in the shear stress. For the laminar average flow, this speedup and the associated decrease in atmospheric pressure above the heap are symmetric for a symmetric heap as is the corresponding shear stress perturbation, which accounts for the dominant symmetric part of $\hat{\tau}$. On the other hand, the inertia of the turbulent velocity fluctuations around this laminar main flow contributes an asymmetric resistance to deflections of the flow. It counteracts the upturn of the streamlines on the windward side and the downturn on the lee side. Formally, this effect enters the perturbative calculation of $\hat{\tau}$ through the Reynolds stress.

Further insight can be gained from special analytical solutions to Eq. (16). For the normalized heap profiles

$$f_L(\xi)=\frac{1}{1+\xi^2},$$

$$f_G(\xi)=\exp(-\xi^2), \tag{22}$$

$$f_C^n(\xi)=S(\xi)\cos^n\xi,$$

with

$$S(\xi)\equiv\begin{cases}1, & |\xi|\leqslant\pi/2\\ 0, & |\xi|\geqslant\pi/2,\end{cases} \tag{23}$$

we obtain

$$\hat{\tau}_L=A(1-2B\xi-\xi^2)f_L^2(\xi),$$

$$\hat{\tau}_G=2A[\pi^{-1/2}-\xi(B+\mathrm{erfi}\,\xi)f_G(\xi)],$$

$$\hat{\tau}_C=\frac{A}{\pi}\cos(2\xi)[\mathrm{si}(\pi+2\xi)+\mathrm{si}(\pi-2\xi)]$$

$$-\frac{A}{2\pi}\sin(2\xi)[\mathrm{ci}(\pi+2\xi)+\mathrm{ci}(-\pi-2\xi)-\mathrm{ci}(\pi-2x)$$

$$-\mathrm{ci}(-\pi+2x)]-2B\,S(\xi)\cos\xi\sin\xi \quad (n=2), \tag{24}$$

with erfi the imaginary error function and si and ci the sine and cosine integral functions, respectively [22]. The result given for $\hat{\tau}_C$ is for the special case $n=2$. A plot of both the profiles of Eq. (22) and the corresponding solutions of Eq. (16) given in Eq. (24) was already presented in Fig. 1 of Ref. [4]. These plots of τ show that as a rule of thumb one can estimate the relative magnitude of the shear stress perturbation at the top of the heap by $A\varepsilon$. They also share several crucial properties that are missing in the affine approximation $\hat{\tau}\propto h$ of the zeroth-order model. At the tails of the profiles, the shear stress falls below its asymptotic value τ_0 on the plane. This effect is most pronounced for the profile f_C^n that has a discontinuity in its second derivative. Further, the surface shear stress is not symmetric even for symmetric profiles like those of Eq. (22). Figure 5 displays the symmetric and asymmetric parts $\hat{\tau}_{\mathrm{sym}}$ and $\hat{\tau}_{\mathrm{asy}}$ of the shear stress perturbation $\hat{\tau}_G$ for the Gaussian profile f_G, separately. The asymmetric contribution to $\hat{\tau}$ is small compared to the symmetric one. For the profile f_L the corresponding shift δx_τ of the location of the maximum of the shear stress with respect to that of the maximum of $f_L(x)$ can be calculated analytically,

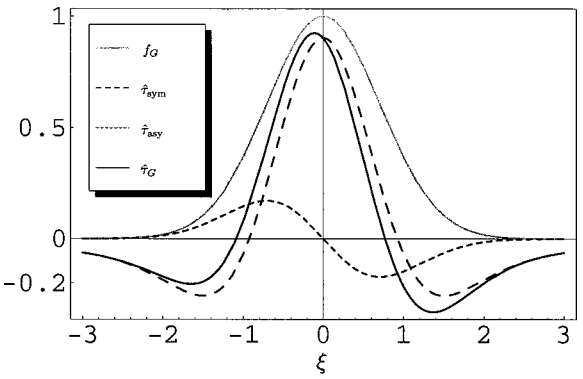

FIG. 5. The symmetric and asymmetric parts $\hat{\tau}_{\mathrm{sym}}$ and $\hat{\tau}_{\mathrm{asy}}$ of the shear stress perturbation $\hat{\tau}_G$ of Eq. (24) for the Gaussian profile f_G of Eq. (22) with $A\varepsilon=0.8$ and $B=0.25$. Note the small windward shift of the maximum of the shear stress with respect to the crest of the heap caused by the asymmetric contribution proportional to B.

$$\delta x_\tau/L=2(1+B^2)^{1/2}\sin[\arctan(B)/3]-B. \tag{25}$$

It is indeed found to be very small, because B is small and thus $\delta x_\tau/L\approx -B/3$ typically amounts to a length of about a few percent of the total heap length. Nevertheless, it is a crucial element in the modeling of aeolian sand transport, as will now be demonstrated.

For a qualitative estimate of the effects of Eq. (16) onto the sand transport over a dune, it is useful to consider once again the local zeroth-order model for aeolian sand transport, Eq. (8), i.e., a completely saturated flux $q=q_s(\tau)$ with q_s given by Eq. (5). (Below, we will show that this is asymptotically valid on large dunes in strong winds.) The distinct features of Eq. (16) that are missing in the zeroth-order approximation for the shear stress, Eq. (7), are then easily seen to have potentially profound effects on the shape evolution. First, due to the depression of the shear stress at the tails of the profiles, deposition rather than erosion may occur at the windward foot. Second, due to the asymmetric contribution in $\tau(x)$ there can be a net deposition on a symmetric heap of sand. In particular, the shift of the position of the maximum shear stress with respect to the top of the heap allows deposition at the top of the heap. For an initially flat heap of sand there is thus the possibility of a steepening of the windward slope and mass growth. This implies that a plane sand surface is unstable against modulations. To illustrate this effect, we used Eq. (24) to calculate the migration velocity $v(x)$ of a cosine-shaped heap of sand $f_C^2(x)$ according to Eqs. (2), (5), (8), and (16). The latter is shown in the upper part of Fig. 6. Since $v'<0$ implies that v increases with height, the decrease of $v(x)$ on the lee side reveals the self-amplifying tendency of the unstable lee slope to steepen, which was already present in the zeroth-order model. It will ultimately lead to the formation of a slip face. In contrast to the zeroth-order model, Eq. (16) however renders $v(x)$ approximately

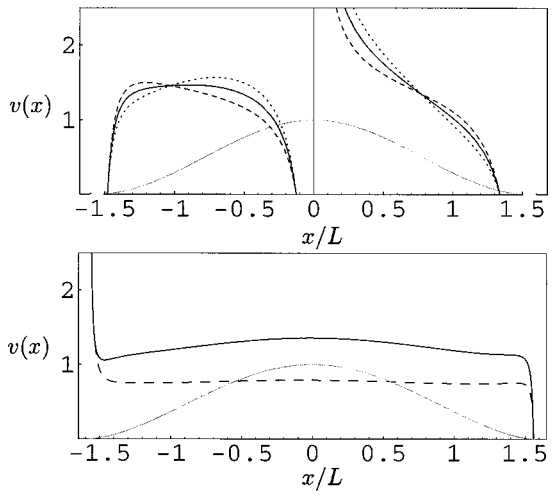

FIG. 6. The position dependent surface migration velocity $v(x)$ in arbitrary units according to Eqs. (2) and (16) with $A=4$, $B=0.25$. Upper part: for the profile f_C^2 (gray) and varying aspect ratios $\varepsilon=0.01$ (dashed), 0.1 (solid), 0.19 (dotted), and the local flux relation Eq. (8). Lower part: for the profile $f_C^{1.65}$ (gray) with $\varepsilon=0.1$ (solid), 0.05 (dashed), and the nonlocal flux relation Eq. (30). To allow direct comparison with the upper part of the figure, q_s was represented by Eq. (5) and $l_s \approx 0.1L$ was taken constant.

constant over almost the whole windward side if $\varepsilon=H/L$ is close to a certain value determined by the values of the coefficients A and B in Eq. (16). Slightly better constancy is possible for a slightly lower n (with slightly larger ε) but *not* for the profiles f_G and f_L, for which $v(x)$ is always nonuniform, so that they are deformed by erosion. Let us finally consider the dashed and dotted lines in the upper part of Fig. 6. They correspond to a smaller and a larger aspect ratio and represent a steepening ($v'<0$) and flattening ($v'>0$) of the windward side, respectively. In other words, profiles with larger/smaller windward slopes are driven towards the solution with constant windward $v(x)$ and a stable optimum windward slope different from zero. Altogether, Fig. 6 thus suggests that the coupled Eqs. (5) and (16) drive a heap of sand towards a dune with a cosinelike windward profile of a preferred aspect ratio, and a slip face on the lee side.

Although the above analysis based on the surface velocity is suggestive, it does not prove that the model converges to a translation invariant steady-state solution if integrated over time. Also some previous studies based on similar descriptions either did not scrutinize the long-time behavior of their models [23,24], or failed to obtain stable dunes [11,25]. However, as our discussion in Sec. II B showed, the long-time behavior is nontrivial and needs special attention. Indeed, the model as developed so far, is still insufficient. To obtain a consistent general model for dune formation under general influx and wind conditions, the present wind model [Eqs. (12) and (16)] has to be appropriately adapted to situations with flow separation above slip faces. And, most importantly, the saturated-flux approximation Eq. (8) of the zeroth-order model has to be abandoned. These steps will be discussed in the following section and in Sec. IV, where we will also explain the lower part of Fig. 6. This will complete the definition of the minimal model. Its numerical solutions will be presented in Sec. V.

C. Flow separation

The wind model as discussed so far works fine for smooth heaps with gentle slopes. However, as we have already mentioned, its application to dune profiles with slip faces and sharp brink lines is not straightforward. The perturbative turbulent boundary layer approach leading to Eq. (12) does not account for flow separation, a phenomenon that occurs at sharp edges and steep slopes to prevent an extreme bending of the streamlines [15]. (For some of the technical terms involved in this section, the reader is referred to Fig. 7.) Instead of bending the streamlines around sharp edges, recirculating eddies separate from the (on average) laminar main flow, thereby creating an effective envelope that diverts the main flow on a smooth detour around the obstacle. See Figs. 7 and 10 for a schematic sketch and a numerical calculation of a typical velocity field, respectively. Fortunately, it turns out that dune formation and migration do not, in general, depend very sensitively on the details of this complicated process. Or in other words, there is a large number of interesting problems of aeolian sand transport for which these details are largely irrelevant, and for which their somewhat realistic physical representation would create a huge overhead in complexity (especially in three dimensions) to an otherwise tractable problem. It was therefore suggested earlier [11] that for the purpose of calculating the shear stress on the windward side of a dune, one may to a good approximation represent flow separation on the lee side by the following heuristic method. A wind model such as Eq. (16) restricted to smooth, gently sloped objects is applied to the envelope

$$\tilde{h}(x)=\max\{h(x),s(x)\} \tag{26}$$

of a dune $h(x)$ and a phenomenologically defined separation bubble $s(x)$. This disregards the fact that the separating streamline does not represent a solid boundary of the same roughness as the original object, but the corresponding errors are expected to be small. Typically, one wants $s(x)$ to be a mathematically simple smooth continuation of the dune pro-

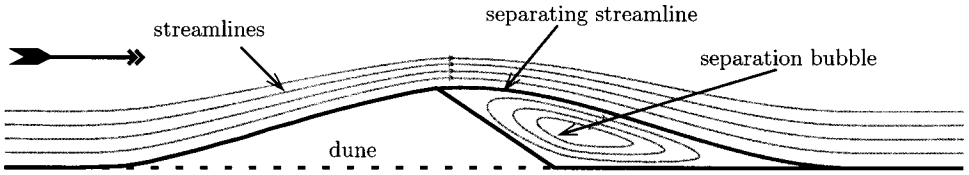

FIG. 7. Sketch of the central slice of a barchan dune and the separation bubble. The shear stress on the windward side of the dune is calculated by applying Eq. (16) to the phenomenologically defined envelope of the dune and the separation zone.

file. It is, however, crucial that the latter respects some major phenomenological properties of flow separation [26]. Although this is by no means a rigorous procedure, one can test its predictions for selected cases against numerical solutions of various turbulence models. The hope is that via this approach, one can eventually get a qualitative understanding of the mechanisms and phenomena involved in dune formation and migration, leaving certain quantitative aspects to a more elaborate (and much more laborious) future analysis.

In the spirit of the minimal model we want to parametrize the separating streamline $s(x)$ in the simplest form that obeys physically motivated boundary conditions at its detachment and reattachment points x_d and x_r. At detachment, the slope of the separating streamline must match the slope of the dune. Moreover, also the curvature must be continuous there, since discontinuities in curvature are detected by Eq. (16) and cause kinks in τ and discontinuous steps in the erosion/deposition, as is, e.g., the case for the profile f_C^2. For the reattachment point, there are no comparable restrictions to the slope and curvature, since the separation bubble is not sharply defined there, and the model aims at a realistic description of the conditions in the wake region only insofar as they affect the shear stress on the *windward* side. On the lee side, inside the separation bubble, the shear stress can simply be set to zero [27], since it is typically below the threshold for aeolian sand transport. Therefore, the choice of the reattachment matching condition is a matter of convenience rather than physical significance in the present model. However, we want $s(x)$ to reproduce some common phenomenological knowledge about flow separation. First, from many numerical calculations it is known that, at high Reynolds numbers, the turbulent boundary layer reattaches at a distance of about $6H$ after a backward-facing step of height H. Second, it has often been observed experimentally that in strongly turbulent flows over hills and symmetric triangular obstacles, flow separation sets in if the backward slope exceeds an angle of about 14°. Although, in both cases the exact numerical values depend on various factors such as the surface roughness and the Reynolds number, they shall be treated as fixed phenomenological constants at the present stage. A model that fulfills all the above requirements is a third-order polynomial with continuous slopes at the boundaries and a maximum negative slope of $\tan 14°$. The boundary conditions

$$s(x_d)=h_d\equiv h(x_d),\quad s(x_r)=0,$$

$$s'(x_d)=h'_d\equiv h'(x_d),\quad s'(x_r)=0, \tag{27}$$

$$\overline{s'}\equiv\max\{-s'(x)\}=\tan 14°=0.25$$

constrain the third-order bubble parametrization to be of the form

$$s(z)=(2h_d+h'_dL_b)z^3-(3h_d+2h'_dL_b)z^2+h'_dL_bz+h_d, \tag{28}$$

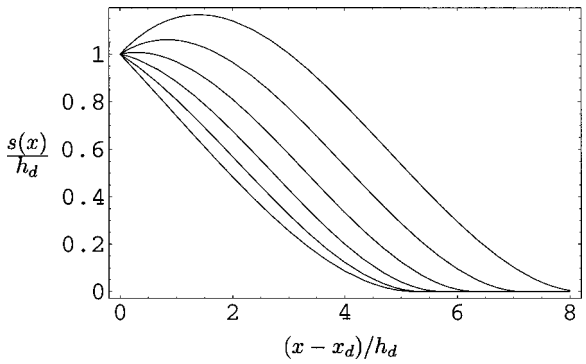

FIG. 8. Separation bubbles with a maximum negative slope of 0.25 according to Eq. (29) for varying initial slopes $-0.25\leqslant h'_d\leqslant 0.25$. (The aspect ratio of the plot was stretched for presentation.)

with $z\equiv(x-x_d)/L_b\in[0,1]$. With the further abbreviation $\nu\equiv h'_d/\overline{s'}$, we can express the length $L_b\equiv x_r-x_d$ of the bubble as

$$L_b=\frac{3h_d}{h'_d}\,\frac{1-\nu-\sqrt{1+\nu}}{3-\nu}\approx\frac{3h_d}{2\overline{s'}}\left(1+\frac{\nu}{4}+\frac{\nu^2}{8}\right), \tag{29}$$

where the final approximation for small h'_d is sufficient for our purpose (and numerically better behaved as the exact expression). A subtlety of such a separation bubble parametrization is the fact that the slope at x_d determines the length of the bubble, which in turn, via Eq. (16) influences the curvature at x_d. In other words, the presence of the bubble introduces a nonlocal feedback between the slope and the curvature at the brink, which we believe is physically reasonable. In Fig. 8 we give some examples of separation bubbles for different boundary slopes h'_d, while Fig. 9 illustrates the application of the above discussion for the calculation of the shear stress. It shows an example for a dune profile $h(x)$ with a slip face and the separation bubble $s(x)$,

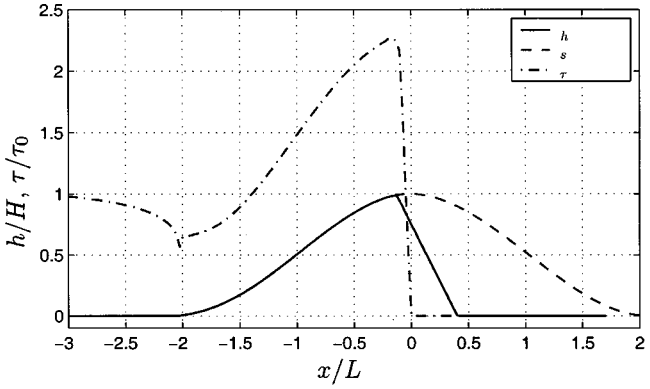

FIG. 9. The windward profile $h(x)$ of a dune with slip face and the separation bubble $s(x)$ form together a smooth effective obstacle, defined by the envelope $\tilde{h}(x)$. To calculate the shear stress $\tau(x)$ on the windward side of the dune, $\tilde{h}$ is substituted for h in Eq. (16). In the region of recirculation the surface shear stress τ is set to zero [27]. Without the separation bubble, $\tau(x)$ would develop a sharp singularity at the brink.

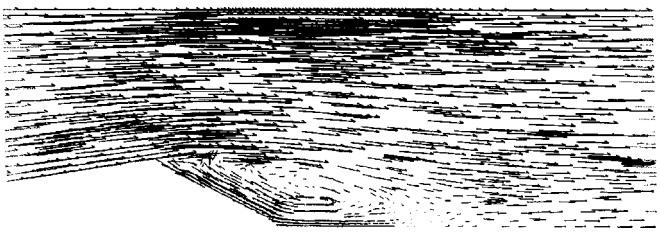

FIG. 10. Cut along the symmetry plane of a 3D barchan dune. The velocity vectors calculated numerically with a commercial fluid dynamics solver [28] clearly display the flow separation at the brink and a large eddy in the wake region.

together with the shear stress $\tau(x)$ resulting from Eq. (16) if h is replaced by the envelope $\tilde{h}$.

We have performed several series of numerical fluid dynamics calculations in two dimensions and three dimensions with the commercial fluid dynamics solver FLUENT5 [28] using the $k\epsilon$ and *large-eddy* turbulent closure models to confirm the general picture outlined above and our particular implementation of the separation bubble. The differences between numerical and theoretical predictions for the shear stress on the windward side of various dunelike and heaplike objects in 2D and 3D were quantitatively small and not more significant than other neglected terms. Moreover, a comparison of predictions obtained from Eq. (28) with wind measurements on a barchan dune in Brazil [29] showed good agreement. Therefore, we are confident that the proposed mathematical description of the wind shear stress captures the relevant aspects in the spirit of the minimal model. As an example for the numerical fluid dynamics calculation, we show in Fig. 10 a section of the flow velocity in the symmetry plane of a 3D barchan dune obtained with FLUENT5 [28]. The wind is blowing from left to right. The boundaries were chosen to be periodic in the transverse direction. At the influx boundary (not shown), the velocity was fixed by imposing a logarithmic velocity profile. The wind profile at the outflux boundary is not known *a priori*. Although, for high Reynolds numbers the latter is expected to affect the solution only close to the boundary, it is well known that different choices for the outflux boundary condition as well as different discretization schemes may lead to quantitatively different results [30]. Here, we chose to set the derivative of the velocity normal to the outflux boundary to zero. The surface profile was represented as a solid boundary with constant roughness length. Finally, along the top boundary we imposed the velocity of the undisturbed logarithmic inflow profile. The whole calculation was performed on a grid that had an exponentially growing mesh size in the vertical direction. A considerable grid refinement was necessary in the wedgelike region of the separation bubble close to the brink.

These remarks complete the first task of constructing a model for the calculation of the wind shear stress on a given dune profile as outlined in Eq. (3). By deriving the linear Eq. (16) for the shear stress and combining it with the heuristic separation bubble, we have obtained an approximate but numerically extremely efficient model for the wind shear stress on dunes. This is a crucial step in the construction of a minimal model of aeolian sand dunes, since the enormous complexity of the turbulent air flow over structured terrain otherwise severely restricts the possible applications of the model.

Going back to the upper part of Fig. 6 with the above discussion in mind, we can reinterpret this figure in order to anticipate the behavior of the surface migration velocity $v(x)$ of a dune with slip face. If, for qualitative purposes, f_C^2 is interpreted as the envelope of a dune and its separation bubble, we can conclude that the slip face must be located near the sharp drop of $v(x)$ slightly upwind from the top of the envelope. This is indeed consistent with observations for large dunes. Together with the good representation of the windward profiles of large dunes [19] by f_C^n $(n \approx 2)$, it suggests that the given description becomes qualitatively correct in the limit of large dune sizes. The following section is devoted to the discussion of important subtleties related to the fact that dunes are not typically in this limit.

IV. SAND FLUX

As outlined in Eq. (4), the second task in the specification of the minimal model is to find a prescription for calculating the sand flux $q(x)$ for a given topography $h(x)$ and shear stress $\tau(x)$. So far, we have been using the local saturated-flux approximation Eq. (8) in our qualitative arguments. However, a closer look at the predictions obtained within this approximation reveals a number of inconsistencies. First, as we have already noted in the discussion of Fig. 6, the use of Eq. (8) together with the complete wind model of Sec. III leads to the odd prediction of deposition at the windward foot of an isolated heap or dune, where the shear stress decreases. This defect of Eq. (8) has been noticed in the literature before (see, e.g., Refs. [8,31]). Previous numerical studies tried to avoid this problem by focusing onto the short-time behavior and by introducing *ad hoc* heuristic methods such as a ''smoothing operator'' [23] or an ''adaptation length'' [24]. The reason for the problem is that the saturated-flux approximation breaks down at the ground-sand boundary. As another shortcoming, we want to mention that the model as discussed so far predicts a universal scale invariant dune shape with a brink that is displaced slightly upwind from the maximum of the envelope, leading always to a positive slope at the brink. A glance at a real dune field proves that the latter is not always the case and careful measurements [19] have revealed systematic deviations from scale invariance. Though less obvious, it turns out that the reason for this discrepancy lies again in the saturated-flux approximation. Both mentioned problems are thus naturally resolved by introducing a slightly more general sand transport law that allows for saturation transients.

A. Saturation transients

The saturated-flux approximation Eq. (8) assumes that the flux is everywhere equal to the equilibrium transport capacity q_s of the wind. However, due to variable wind or sand conditions, the actual sand flux q is, in general, different from q_s. These deviations are called saturation transients, because they quickly relax to zero under homogeneous con-

ditions. We have recently demonstrated [8] that this relaxation occurs within a characteristic length scale, called the *saturation length* ℓ_s, which is related to (but distinct from) the mean saltation length of the grains. It was, moreover, shown how the introduction of saturation transients cures the problem of deposition at the windward foot of an isolated sand dune. Here, we only summarize the most pertinent results of this earlier development in order to demonstrate how a size dependence of the dune shape naturally results as a consequence of saturation transients.

The sand transport model of Ref. [8] is based on a mean-field-like description of saltation. It models a typical grain that is accelerated by friction with the air and slowed down by dissipative interactions with the bed. The average properties of the complicated splash process [32–34] are subsumed into two dimensionless parameters, an effective restitution coefficient α for collisions with the bed, and a kinetic coefficient γ that characterizes the relaxation of the density of saltating grains to its saturated value. Together with an effective height for the wind-grain interaction that enters only logarithmically, these are the only phenomenological parameters of the model. They have been determined by a comparison with experiments and grain scale simulations. Formally, the model consists of two coupled differential equations for mass and momentum conservation, and a modified turbulent closure relation that accounts for the feedback of the saltating grains on the wind velocity.

For the present purpose, the model can be simplified by taking advantage of the fact that the prevailing conditions in applications to dunes are typically well described by the steady-state ($\partial/\partial t \simeq 0$) version. Further, the relaxation of the typical sand transport velocity can be assumed to be fast compared to the variations in the density of mobilized grains in the saltation layer. Approximating the latter by its saturated value for the calculation of the effective wind speed u_{eff} via the modified turbulent closure, one can decouple the mass and momentum conservation equations. The whole model can then in a reasonable approximation be reduced to a single differential equation

$$\ell_s \partial q/\partial x = q(1-q/q_s) \tag{30}$$

for the sand flux $q(x)$. The shear stress dependent parameters

$$\ell_s = l/(\tau/\tau_t - 1), \quad q_s = \rho_s u_s \tag{31}$$

are immediately identified as the saturation length and the saturated flux, respectively. The equation for q_s generalizes Eq. (5) to arbitrary wind speeds. In the following we specify the explicit expressions for both quantities as they result from the sand transport model of Ref. [8], but the structure of Eq. (30) is thought to be more general and independent of the precise form of Eq. (31). Again, $\tau(x)$ is the position dependent shear stress discussed in Sec. III and $\tau_t \approx 0.1\ \mathrm{kg\,m^{-1}\,s^{-1}}$ is the estimated impact shear stress threshold that corresponds to a critical shear velocity $u_{*t} \approx 0.28\ \mathrm{m\,s^{-1}}$ [35]. (For simplicity, we do not introduce the additional threshold for purely aerodynamic entrainment here, but allow instead for a small residual influx even if the latter is nominally zero.) To make the underlying structure of the model more palpable, we have expressed ℓ_s in terms of another characteristic length scale $l \equiv 2\alpha u_s^2/(g\gamma)$, which (up to a numerical factor) is the average saltation length of the grains. The latter—but not ℓ_s—must always be considerably smaller than the dune length for the model to be applicable. Further, we have decomposed q_s into the saturated density $\rho_s = 2\alpha(\tau-\tau_t)/g$ and the effective sand transport velocity at saturation $u_s = u_{\mathrm{eff}} - \delta u$ with u_{eff} the effective wind velocity that accelerates the grains, given by

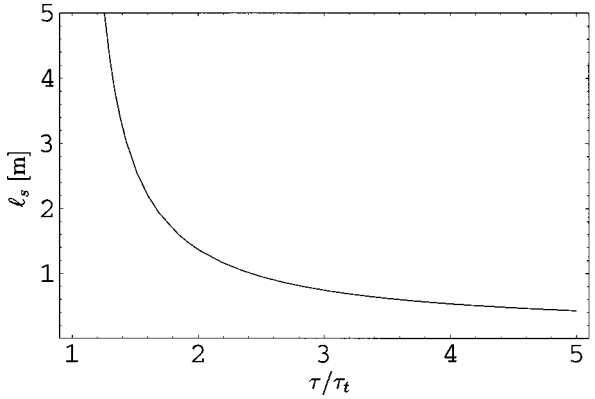

FIG. 11. The saturation length ℓ_s in meters as a function of the shear stress exerted by the wind onto the sand bed. This function sets the natural length scale for dunes and heaps.

$$u_{\mathrm{eff}} \kappa \sqrt{\varrho_a} = 2\sqrt{\tau_t + (\tau-\tau_t)/\zeta} + (\ln \zeta' - 2)\sqrt{\tau_t}. \tag{32}$$

By g we have denoted the gravitational acceleration and from Ref. [8] we adopt the (approximate) numerical values $\alpha = 0.35$, $\gamma = 0.2$, $\zeta = 8$, $\zeta' = 200$, and $\delta u = 1.8$ m/s for the lag velocity of the grains. We note that these numerical values are not completely independent of each other and of the mentioned value for the impact threshold τ_t, due to the calibration of the sand transport model with experimental data [8]. For convenience we show a plot of the saturation length ℓ_s obtained with these values in Fig. 11. This completes the definition of the sand transport part of the minimal model on gently sloped ground.

B. Consequences

Before we complete the general model definition by a brief paragraph on slip faces, we want to point out some implications of the model as developed so far. First, note that the full expression for q_s given in Eq. (31) contains Eq. (5) as a limiting case for strong winds but is better approximated by $q_s \propto \tau - \tau_t$ for moderate wind speeds. For weak flux gradients and strong winds, one may set the left hand side of Eq. (30) to zero, leading to $q = q_s$. This is typically the case on most of the windward slope of a large dune, where the left hand side of Eq. (30) can roughly be estimated by $\ell_s q_s/L \ll q_s$. The local saturated-flux approximation with Eq. (5) for q_s, which we have applied throughout our qualitative discussion so far, is thus asymptotically valid for large dunes and strong winds (except near the windward foot of an isolated dune). This is what one might have expected in the first

place, and the reader may wonder at this point how the saturation transients and their characteristic length scale ℓ_s can have the claimed importance. How can ℓ_s affect the shape of a dune that is typically about two orders of magnitude larger? This apparent puzzle is now easily resolved by going back to Fig. 5 and Eq. (25) and by observing that the symmetry breaking shift δx_τ of the location of the maximum of the shear stress with respect to that of the maximum of the height profile (or envelope), which is responsible for the finite windward slope and growth of dunes, is also of the order of a few percent of the total dune length. In summary, the longitudinal profile of dunes and heaps is determined by the competition of two quantitatively small but qualitatively crucial effects, one related to turbulent wind flow and the other to sediment transport. This may be the reason why its explanation proved elusive for a long time.

To get a qualitative idea of the consequences of the introduction of the generalized nonlocal flux law in Eq. (30) as a replacement for Eq. (8), we want again to go back to our discussion of the surface migration velocity of the cosine-shaped heap f_C^n in Fig. 6. Let us for the moment adopt a crude approximation and replace the expression for q_s given in Eq. (31) by its simpler limiting form $q_s \propto \tau^{3/2}$ introduced in Eq. (5) for reasons of comparison. For the same reason, we also neglect the variation of ℓ_s on the dune and replace it by a (fine tuned) constant $\ell_s \approx 0.1L$. With an influx (about $0.7q_s$ for the solid and $0.8q_s$ for the dashed line in the lower part of Fig. 6) one can thus achieve a fairly constant surface velocity over the *whole* length of a cosine-shaped heap. Again the constancy is slightly better for $n<2$ than for $n=2$. It is further improved by reducing the slope of the heap well below the optimum windward slope of the dune obtained for $\ell_s \to 0$, as seen from a comparison of the solid line and the dashed line. We also note in passing that the influx needed to maintain the shape is increasing with decreasing slope. The comparison of the uppper and lower part of Fig. 6 confirms our claim that even for $\ell_s \ll L$, saturation transients may visibly affect the overall shape of aeolian dunes. Although, for the example shown in the lower part of Fig. 6, the saturation length is only about 1/30 of the heap length, the slip face instability is evidently completely washed out. Altogether, this strongly suggests the existence of translation invariant cosine-shaped heap solutions for the model. The ultimate proof will be provided by the numerical results presented in Sec. V, where the full form of q_s and ℓ_s according to Eq. (31) will be used, but the present crude approximation already illustrates the main point, and also demonstrates that the behavior is a generic consequence of Eq. (31) and insensitive to the detailed form of the parameters $\ell_s(x)$ and $q_s(x)$ that may phenomenologically be somewhat different from the model prediction without affecting our general conclusions.

An immediate consequence of the foregoing discussion is the existence of a minimum dune size. For small enough dunes, the slip face instability is washed out by the saturation transients. One may also arrive at this conclusion from an analysis of heaps. To this end we observe that the value of the saturation length ℓ_s is a property of the wind velocity and the saltation kinetics and depends on the topography only indirectly through the variable shear stress τ. Moreover, it is apparent from Fig. 11 that this dependence becomes weak for strong winds. On the other hand, the symmetry breaking shift δx_τ is proportional to the absolute size of the heap (or envelope) and not directly dependent on the wind velocity. For the special profile f_L, this was verified analytically in Eq. (25). As we have seen, a smooth heap can only be a translation invariant solution of the model if the lag (of order ℓ_s) of $q(x)$ with respect to $q_s(x)$ and the shift δx_τ are fine tuned to guarantee a vanishing erosion rate at the top of the heap. From this we expect heaps to obey

$$\ell_s \simeq \delta x_\tau \propto L \approx \text{const} \tag{33}$$

to a first approximation. This condition can only be fulfilled if the aspect ratio ε of heaps grows proportional to their size (i.e., roughly $\varepsilon \propto H$). Hence, in contrast to large dunes with slip face, for which we have argued that they are asymptotically scale invariant ($\varepsilon \sim \text{const}$), heaps must have a strongly size dependent aspect ratio. As a consequence, translation invariant heap solutions obviously cannot exist beyond a certain critical size. A slip face will develop when the shear stress on the lee side of the heap drops below the threshold value τ_t, or at the latest, when the lee slope exceeds the critical slope for flow separation. This will be further analyzed in Sec. V. Finally, we note that the steady-state flux of a heap can be estimated by the observation that the outflux is essentially determined by the strength of the reduction $\tau_0 - \tau_{\min}$ of the shear stress at the lee end of the heap. According to Eq. (9), the latter is (for a given shape) proportional to the aspect ratio ε. For qualitative purposes, the outflux q^{out} may thus be estimated in the saturated-flux approximation with Eqs. (31), (32), and (9) as

$$q_s^{\text{out}} \propto \tau_{\min} - \tau_t \propto \varepsilon_c - \varepsilon, \tag{34}$$

where we have assumed $\tau_{\min}/\tau_t \lesssim 2$ (fulfilled for moderate wind speeds and/or heaps near the critical heap size) to linearize the expression for $q_s(\tau)$ given in Eq. (31). Here, $\varepsilon_c \propto \tau_0 - \tau_t$ is the critical aspect ratio for which the shear stress on the lee drops below the threshold and the outflux vanishes. Note that the latter increases with increasing shear stress whereas the heap length decreases according to Eqs. (31) and (33). The effects of the two trends onto the critical heap mass could therefore partially cancel unless the lee slope exceeds the critical slope for flow separation.

C. Slip face

We have argued above that for large heaps ($L \gg \ell_s$), aeolian sediment transport tends to increase the downwind slope until it reaches the angle of repose of the grains. At this point, any further increase of the lee slope initiates avalanches that restore a slope slightly below the static angle of repose and eventually create a slip face of a roughly uniform slope of about 32°–35°. Since the physical modeling of this process itself is not a major objective of the present contribution, we can choose between different possible implementations for this phenomenon. In 2D it is possible to represent the slip face as boundary condition for the sand transport. It

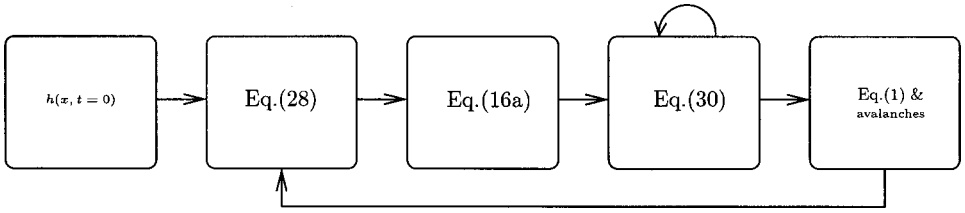

FIG. 12. Solution of the minimal model.

is uniquely determined by its fixed uniform slope and mass conservation. However, with regard to a future generalization of the present 2D model to three dimensions we chose a more realistic implementation based on a widely used avalanche model [36]. The formulation of this model bears some close similarities with the sand transport model presented in the preceding paragraph, and thus suggests itself as a natural extension of the latter to the slip face. This completes the definition of the minimal model that will be solved numerically in the following section.

V. SOLUTION OF THE MODEL

Apart from the model definition, the preceding sections have provided some qualitative insights into the main mechanisms responsible for dune formation and migration. Now we are prepared to study numerically the quantitative predictions of the model. Again, we emphasize that we only can explore some major features of the model in the present report, leaving many interesting questions and more systematic and quantitative parameter studies for future work.

For convenience, the solution procedure of the minimal model is summarized as a flowchart in Fig. 12. One starts with an initial profile $h(x,t=0)$ (typically f_G or f_C^2), checks whether a separation bubble has to be added for the calculation of the shear stress, then obtains the latter from Eq. (16a) and uses the result as input for the iterative solution of the sand transport equation Eq. (30). This finally gives the erosion/deposition needed to update the surface profile. Technically, Eq. (16a) is implemented as a fast-fourier-transform algorithm, and for the integration of Eqs. (30) and (1) an upwind discretization scheme is used. Simulation times can be reduced by using an adaptive time step.

A. Steady-state shapes

The scheme of Fig. 12 can be iterated for different influx boundary conditions. For all of the numerical calculations presented below, we chose periodic boundary conditions. They are the natural choice for studies of the steady-state shapes. To investigate the mass balance under prescribed influx conditions, on the other hand, one has to apply open boundary conditions.

Figure 13 shows steady-state solutions of the model for initial profiles f_G of different mass. These solutions are obtained for fixed wind conditions with parameters $A=3.2$ and $B=0.25$, appropriate for the central slice of a 3D (symmetric) heap or of a barchan dune. The shear velocity $u_*=0.4$ m/s lies well above the impact threshold. (The situation very close to or below the threshold would need special attention.) As anticipated above, large dunes become asymptotically scale invariant. The asymptotic master curve for the windward profile is practically indistinguishable from the profile f_C^n ($n \lesssim 2$), and the slope at the brink is indeed positive. Its average windward slope is inversely proportional to the value of the parameter A given in Eq. (13). Due to the additional terms in the expression Eq. (18) for the shear stress on dunes with a finite width, somewhat steeper average windward slopes are predicted for barchan dunes than for transverse dunes under identical influx and wind conditions. A detailed quantitative comparison is probably beyond the scope of the present semi-quantitative implementation. More important are the remarkable qualitative predictions of the model. In particular, the fact that dunes with a slip face are only stable above a certain (wind dependent) critical size, whereas smooth steady-state heaps only exist below a critical size, deserves attention. We also note that the steady state is not always unique. There is a hysteretic regime where the initial conditions can select one of two possible steady-state shapes and accordingly the masses for the two sets of profiles in Fig. 13 are not all distinct. The largest heaps in the upper plot were obtained from flat initial profiles f_G, whereas the smallest dunes with a slip face in the lower plot were obtained from steeper initial profiles f_G of the same mass. Especially, the dune with a negative slope at the brink could only be obtained from steep initial conditions. Since under natural wind and sand conditions, the initial conditions themselves will generally be heaps or dunes close to the steady state, one can say that the model predicts a critical heap size for slip face formation and a critical dune size for slip face destruction. In both cases the slip face is finite as a conse-

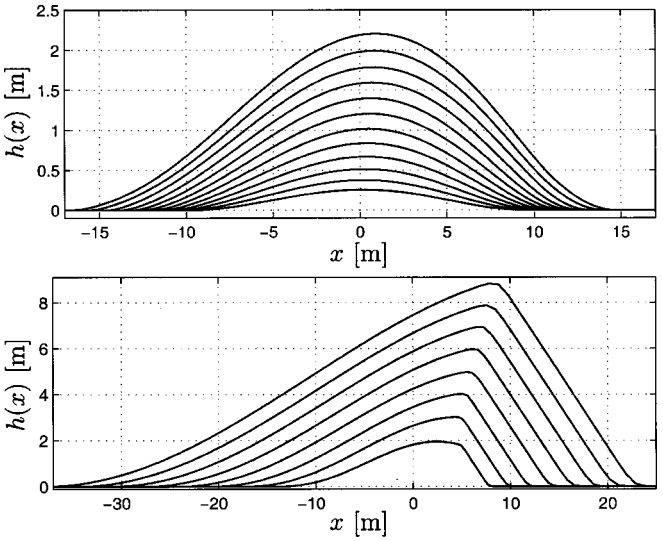

FIG. 13. Steady-state heaps (upper plot) and dunes (lower plot). The aspect ratio is stretched for better visualization.

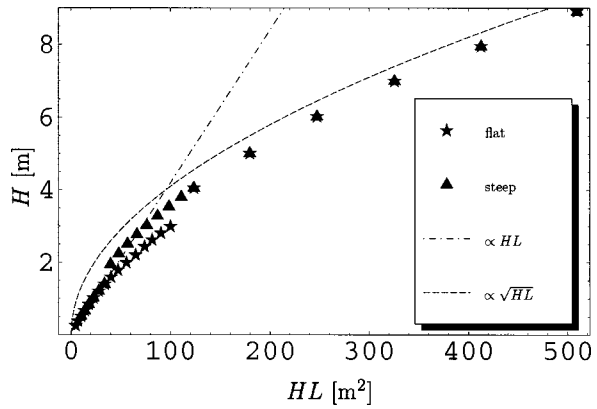

FIG. 14. Steady-state heights H versus the product of the height and length of the heaps and dunes. In the hysteretic regime, flat and steep initial conditions have to be distinguished.

quence of flow separation. The latter also allows a dune to be somewhat higher than a heap of the same mass, since its effective volume as seen by the average air flow is increased by the separation zone. As anticipated, the aspect ratio of the dunes is asymptotically constant, whereas it is strongly size dependent for heaps. This effect can be seen more quantitatively in the representation of Fig. 14, where the height H of the steady-state heaps and dunes is plotted versus the product HL of their height and length L. Clearly, heaps are better described by $H \propto HL$ as predicted in Eq. (33), whereas large dunes approach the scaling limit $H \propto \sqrt{HL}$.

B. Migration velocity

For the overall migration velocity of steady-state dunes with a scale invariant profile, we derived on general grounds, the simple scaling prediction $v \propto L^{-1}$ in Sec. II C. We have also given some arguments why this prediction should be rather robust against relaxing the condition of shape invariance, in contrast to the relation $v \propto H^{-1}$ that can only be inferred from it if the scaling assumption holds exactly. Here, we check these predictions for the steady-state solutions numerically. Figure 15 shows the numerically obtained migration velocity for dunes fitted to the scaling relations $v \propto H^{-1}$ (left) and $v \propto L^{-1}$ (right). As we have mentioned above, one has to take for L the characteristic length of the envelope rather than that of the dune alone. For simplicity, we estimate L by adding $6H$ to the horizontal length from the windward foot of the dune to its crest, thus neglecting the weak slope dependence of the size of the separation bubble. Obviously, the L^{-1} scaling is superior for moderate winds and small dunes, where $v \propto H^{-1}$ systematically fails to describe the data. This is also supported by field data [21]. Both fits become identical in the scaling limit $L \gg \ell_s$. Due to the decrease of ℓ_s with the wind speed, the latter is reached for smaller dunes at stronger winds.

C. Stability

We have already pointed out that the choice of different boundary conditions for the flux allow a separate discussion of shape and mass stability. This is of practical importance, since (in two dimensions) all steady-state shapes are unstable with respect to mass changes. If the influx of a steady-state solution deviates slightly from its corresponding steady-state flux, this solution will start to either shrink until it has flattened out or grow without bound. Despite the fact that the steady-state shapes are (locally) stable attractors for the shape evolution under periodic flux conditions, mass stability can, in general, not be achieved under open boundary conditions. The situation is clarified in Fig. 16. It depicts the steady-state sand flux q over the bedrock as a function of the aspect ratio. The numerical results nicely confirm our theoretical expectation from Eq. (34). For all dunes with slip face the flux vanishes identically in two dimensions, whereas in general it grows with decreasing size for smooth heaps. For open boundary conditions, the line in Fig. 16 can be interpreted as an unstable phase boundary (with hysteresis) between infinitely growing and shrinking solutions. For example, a heap with influx slightly below the steady state will shrink a bit. To remain close to the steady-state shape, it will therefore mainly reduce its height, whereas its length will stay almost constant. Due to the reduced aspect ratio ε, $\hat{\tau}$ decreases in magnitude and the shear stress depression at the lee boundary is less pronounced. As a consequence there is

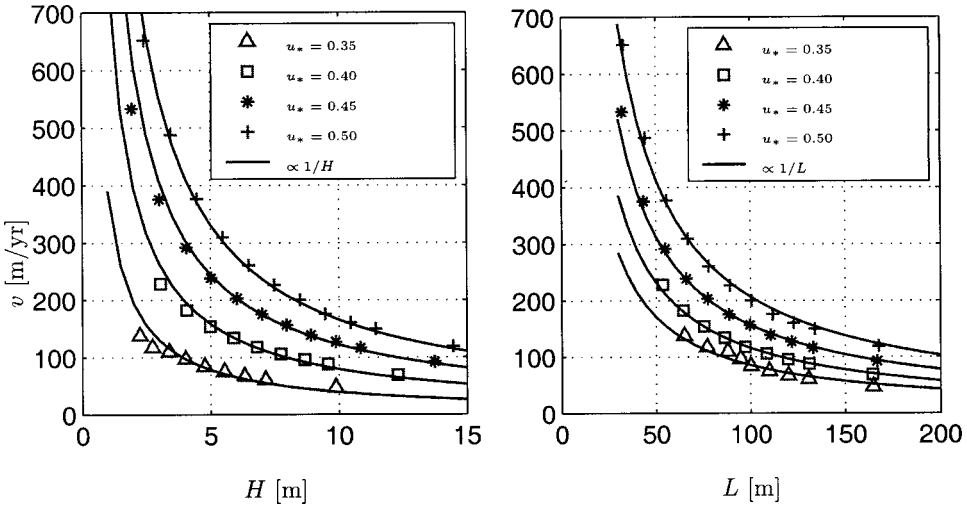

FIG. 15. Migration velocities predicted by the minimal model for steady-state dunes of different size at various wind velocities. The caption gives the shear velocity u_* in m/s. The numerical data are compared to the scaling laws $v \propto H^{-1}$ (left) and $v \propto L^{-1}$, where L is the length of the envelope of the dune and its separation bubble as described in the main text. (Note that the migration of real dunes is substantially slower due to the small fraction of wind days per year.)

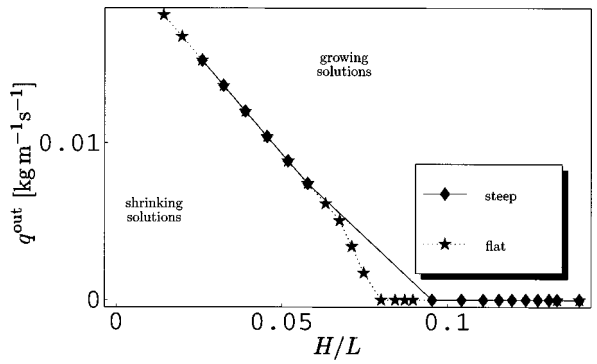

FIG. 16. Steady-state outflux under periodic boundary conditions. In the hysteretic regime, steep and flat initial conditions have to be distinguished, as in Fig. 14. The figure may also be read as a phase diagram for the situation with open boundary conditions. In this case the steady-state solutions—though attractors for the shape—are unstable with respect to mass fluctuations.

less deposition on the downwind slope and the outflux is higher, so that the heap shrinks even more, etc. A completely analogous reasoning applies to the opposite case of higher influx.

The above discussion explains why isolated smooth aeolian sand heaps are rarely observed as distinct features of desert topographies. Under approximately stationary wind and influx conditions they only exist as transient states that either vanish or develop into dunes with a slip face. Under variable wind and influx conditions, the situation is less clear and deserves a detailed study of its own. For example, the model predicts that during a period of strong wind all dunes are driven towards the asymptotic shape. After a subsequent period of weak winds, finite size effects become more pronounced, and small dunes may develop longitudinal profiles such as those in the hysteretic regime or even loose their slip face. Again, the case $\tau_0 \approx \tau_t$ of a shear stress close to or below the threshold shear stress needs special attention.

The prevailing wind conditions as well as recent changes in the wind velocity are thus encoded in a complicated but comprehensible way in the shapes of the dunes in a dune field. This is a promising direction for further studies. One may hope that by systematic studies along these lines one will in the future be able to infer flow conditions in remote or uncomfortable places (e.g., on the sea bottom or on other planets [37,38]) by analyzing dune shapes.

D. Relaxation dynamics

As a first step towards an understanding of the effects of variable wind speeds (for constant wind direction), this section is devoted to an exploratory study of the transient shape evolution. We restrict ourselves to periodic boundary conditions leaving the richer phase space of open boundary conditions for future studies. Figure 17 shows two extreme scenarios. A flat initial condition with a mass greater than the critical mass for slip face formation in the upper two panels, and a steep initial condition of the same mass in the lower panel. The steep initial condition quickly leads to the formation of a slip face, whereas the flat heap needs to steepen for

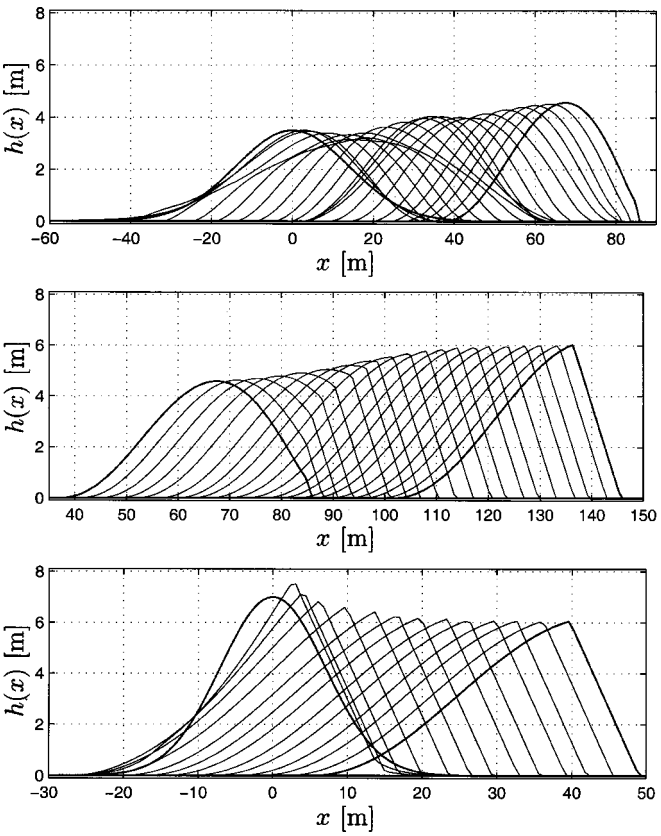

FIG. 17. Upper two panels: growth history for a Gaussian heap of longitudinal aspect ratio $H/\sigma = 1/4$. Lower panel: growth history for a Gaussian heap of the same mass but longitudinal aspect ratio $H/\sigma = 1$. Both initial conditions converge to the same steady-state shape. The shear velocity was fixed to $u_* = 0.45$ m/s for both simulations.

a long time until the shear stress on the lee falls to the threshold value. This causes complete deposition on the lee side of the heap and thus leads to slip face formation. Whether this happens before or with the onset of flow separation depends on wind and influx conditions. As it also depends on the precise numerical values of some of the phenomenological parameters of the model, a detailed parametric study is again beyond the scope of the present contribution.

Although the times to reach the steady state are apparently somewhat longer for the flat initial condition, it is evident from Fig. 17 that the relaxation dynamics is in general relatively fast even if the initial condition is far from the steady-state shape. Large dunes under low influx conditions as they prevail, e.g., in fields of isolated dunes should therefore be well described by an adiabatic approximation, assuming that (except after drastic changes in the wind and sand conditions as they occur during sand storms) the dune is practically in a steady state. Apart from the low influx, this also relies on the fact that virtually no sand is lost over the slip face. For a large isolated 3D barchan dune this implies that most of the sediment transported over the dune is actually trapped in a treadmilling flux, and only a small portion of the total flux is contributed by and contributes to the external flux. Hence, under steady wind conditions these dunes are in a quasisteady state and thus very close to their true

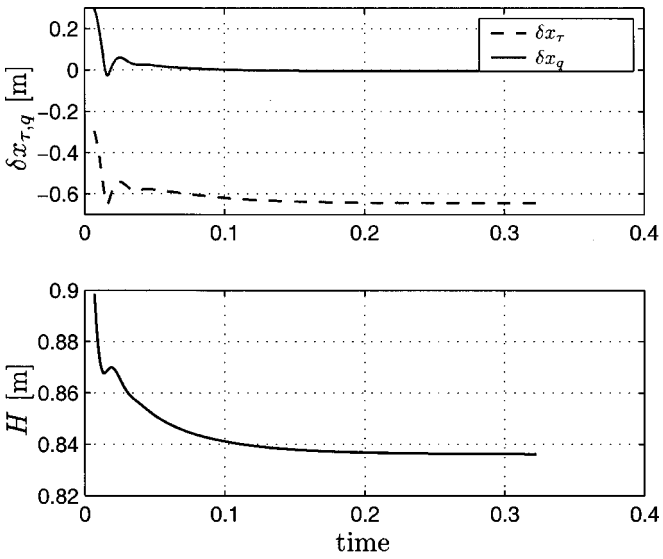

FIG. 18. The figure shows the transient evolution of various interesting length scales for a heap. Lower part: height of the heap. Upper part: distance of the locations of the maximum of the shear stress and of the maximum of the sand flux from the position of the top of the heap. In the steady state, the erosion/deposition vanishes at the crest.

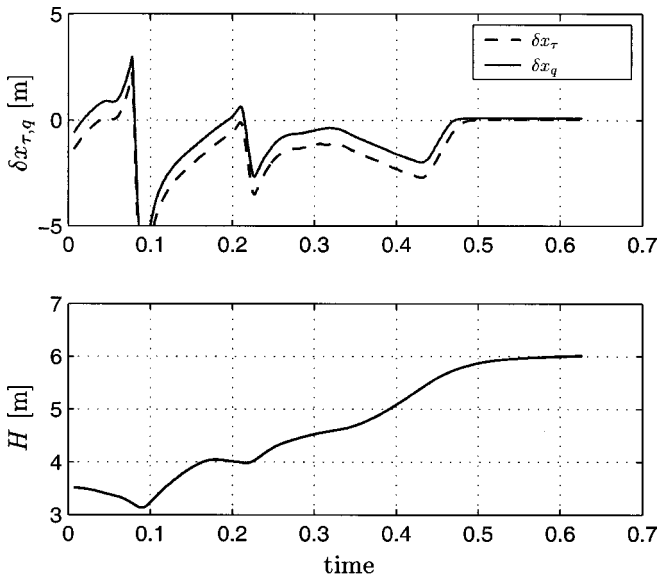

FIG. 19. The figure shows the transient evolution of various interesting length scales for a dune that develops out of a smooth heap as in the upper pannel of Fig. 17. Lower part: height of the dune. Upper part: distance of the locations of the maximum of the shear stress and of the maximum sand flux from the position of the top of the crest. The lag between shear stress and sand flux vanishes when the slip face reaches the crest.

steady-state shape. Investigation of the steady-state properties is therefore the starting point also for the study of their time evolution. Moreover, this suggests that a comparison of our steady-state shapes to shapes obtained in field measurements is justified. In fact, the calculated shapes agree nicely with recent measurements for barchan dunes [19]. The situation is less clear for small heaps, where mass losses can be of the order of the total flux and may thus lead to significant differences between the steady-state and the transient shapes under vanishing influx.

In the remainder of this section, we want to investigate more closely the mechanism that drives the shape relaxation. As we have pointed out, the positions of the maximum of the sand flux and of the maximum of the profile must coincide in the steady state to make the erosion/deposition vanish at the crest. We have shown that for small heaps, this can be achieved by a fine tuning of δx_τ to about ℓ_s. In contrast, for large dunes and strong winds, $\delta x_\tau \gg \ell_s$ and the steady-state condition can only be met with a singularity at the crest. This important difference is exemplified by Figs. 18 and 19. Both figures show the evolution of the height and the displacements, δx_τ and δx_q, of the locations of the maximum of the shear stress and of the maximum of the sand flux from the location of the top of the sand profile, respectively. The distance between both displacements is the lag of the flux with respect to the shear stress due to the saturation transients, and is therefore closely related to the saturation length ℓ_s for smooth surface profiles. It guarantees the proper vanishing of the erosion rate q' at the top of a steady-state heap where δx_τ is finite, but vanishes for large steady-state dunes, where the slip face ends in a sharp brink singularity at which the grains fall into the wake and are quickly deposited.

VI. SUMMARY AND OUTVIEW

In summary, we have shown that a simple minimal model for the wind-driven sediment transport over a sand dune is capable of explaining several important features of desert topographies. Among them are the migration velocities of heaps and dunes, their shape along the wind direction, and the existence of a minimal dune size and a maximum heap size.

As we have emphasized throughout this contribution and demonstrated by the numerical solutions in the preceding section, the symmetry breaking part of the shear stress exerted by turbulent air flow on an obstacle, and local deviations of the sediment flux from its equilibrium transport capacity (''saturation transients''), are the essential ingredients in the modeling of aeolian sand dunes. It is exactly the balance of these two relatively small effects that is responsible for the relaxation of arbitrary initial conditions into a characteristic dune or heap shape. Their neglect was responsible for the failure of the naive zeroth-order model discussed in Sec. II B. In hindsight we can say that it is not so much the quantitative errors but the omission of this *qualitatively* important mechanism that makes the zeroth-order model an insufficient description. In contrast, taking this balance properly into account makes the minimal model structurally stable against the neglect of less significant quantitative details of the same order of magnitude.

This direction was recently pursued further in an effort to calculate analytically certain steady-state shapes of dunes and heaps by ''linearizing'' the minimal model [39]. One may as well wish to proceed also into the opposite direction. After the basic mechanism is understood, more elaborate

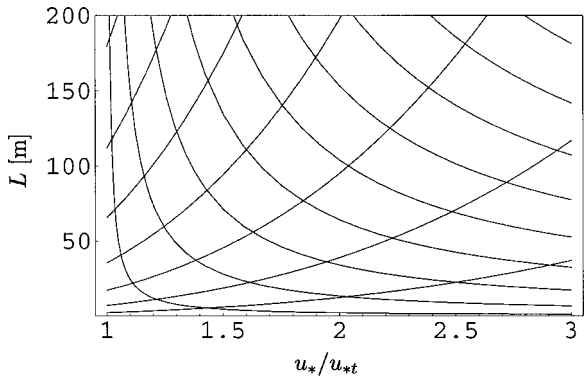

FIG. 20. Qualitative shape diagram that could be useful in the analysis and comparison of field studies. The migration velocity is constant along rising lines, whereas falling lines indicate invariant dune shape.

dune models can be constructed by putting some of the neglected details back into the description. Detailed parametric studies of such a refined model for a certain dune type and comparison to field data would be very useful to test some of the less generic predictions of the underlying sand transport model [8], such as the shear stress dependence of the saturation length ℓ_s (Fig. 11). This is important, since, as we have shown, the variable parameter ℓ_s sets the characteristic length scale with respect to which dunes and heaps can be said to be large or small. Phenomenological knowledge about ℓ_s is still very limited. More detailed studies could further be helpful to map out quantitative shape diagrams, of the type sketched qualitatively in Fig. 20. These diagrams could be useful not only for the validation of the model, but also for the comparison of field data from different places with different prevailing wind and sand conditions. The migration velocity is constant along the rising lines in Fig. 20, which were obtained from Eq. (11) using $q \approx q_s$ together with Eq. (31). They allow, for example, a comparison of the migration velocities of dunes of different sizes that are exposed to (on average) identical winds. Or one may infer the average wind speed from measurements of sizes and migration velocities in a dune field. The falling lines in Fig. 20 are lines of constant shape, assuming that the latter is determined by ℓ_s/L, which holds for the steady state. They may thus be used for correlating wind speeds with dune shapes. In general (in particular, for the full 3D problem), such shape diagrams will be more complex since the influx is an additional important variable that we have neglected here, as it vanishes for 2D dunes in the steady state.

Moreover, as we pointed out, there are still many consequences of the present model that await a systematic investigation. And a major future task is finally the generalization of the present discussion to the 3D case. A promising route could be the construction of an effectively sliced model that allows one to use the proposed model for the separation bubble and to keep the time-limiting calculation (the integration of the flux equation) effectively one dimensional. The smaller transverse currents could be inferred from the sliced solution. A generalization of the flux equation to the 2D surface of a 3D dune is also feasible [29]. A more ambitious task will eventually be the simulation of dune fields. Whereas the existence of a minimum dune size could be obtained by an analysis of the shape stability alone, the question of a possible existence of a characteristic or maximum dune size in a dune field depends on the mass balance of a dune in the complicated environment provided by the other dunes, and is much more difficult to answer [40].

ACKNOWLEDGMENTS

We thank Ken Andersen and Philippe Claudin for helpful discussions, and acknowledge financial support by the Deutsche Forschungsgemeinschaft (Contract No. HE 2732/1-1) and by the European Community (K.K.).

[1] R. A. Bagnold, *The Physics of Blown Sand and Desert Dunes* (Methuen, London, 1941).
[2] K. Pye and H. Tsoar, *Aeolian Sand and Sand Dunes* (Unwin Hyman, London, 1990).
[3] N. Lancaster, *Geomorphology of Desert Dunes* (Routledge, London, 1995).
[4] K. Kroy, G. Sauermann, and H.J. Herrmann, Phys. Rev. Lett. **88**, 054301 (2002).
[5] R.B. Hoyle and A.W. Woods, Phys. Rev. E **56**, 6861 (1997).
[6] R.B. Hoyle and A. Mehta, Phys. Rev. Lett. **83**, 5170 (1999).
[7] L. Prigozhin, Phys. Rev. E **60**, 729 (1999).
[8] G. Sauermann, K. Kroy, and H.J. Herrmann, Phys. Rev. E **64**, 031305 (2001).
[9] P.S. Jackson and J.C.R. Hunt, Q. J. R. Meteorol. Soc. **101**, 929 (1975).
[10] R.I. Sykes, J. Fluid Mech. **101**, 647 (1980).
[11] O. Zeman and N. O. Jensen, Risø National Laboratory, Technical Report No. M-2738, 1988 (unpublished).
[12] J.C.R. Hunt, S. Leibovich, and K.J. Richards, Q. J. R. Meteorol. Soc. **114**, 1435 (1988).
[13] D. J. Carruthers and J. C. R. Hunt, in *Atmospheric Processes over Complex Terrain*, edited by W. Blumen (American Meteorological Society, Boston, 1990), Vol. 23.
[14] W.S. Weng, J.C.R. Hunt, D.J. Carruthers, W.A. , G.F.S. Wiggs, I. Livingstone, and I. Castro, Acta Mech. (Suppl.) **2**, 1 (1991).
[15] Landau and Lifshitz, *Fluid Mechanics*, Course of Theoretical Physics Vol. 6 (Pergamon Press, London, 1963).
[16] *Aeolian Grain Transport 1 & 2*, edited by O. E. Barndorff-Nielsen and B. B. Willetts Acta Mechanica Supplement (Springer, Wien, 1991).
[17] K. Lettau and H. H. Lettau, in *Exploring the World's Driest Climate*, edited by H. H. Lettau and K. Lettau (Center for Climatic Research, University of Wisconsin, Madison, 1978).
[18] M. Sørensen, Acta Mech. (Suppl.) **1**, 67 (1991).
[19] G. Sauermann, P. Rognon, A. Poliakov, and H.J. Herrmann, Geomorphology **36**, 47 (2000).
[20] This has to be distinguished from the statement that the migration velocity of a dune with a slip face is proportional to the flux over the brink divided by the height, which is (trivially)

true if losses over the slip face are negligible, but useless unless the flux over the brink is specified.
[21] H.J. Finkel, J. Geol. **67**, 614 (1959).
[22] M. Abramowitz and I. A. Stegun, *Handbook of Mathematical Functions* (Dover, New York, 1965).
[23] F.K. Wippermann and G. Gross, Boundary-Layer Meteorol. **36**, 319 (1986).
[24] P.M. van Dijk, S.M. Arens, and J.H. van Boxel, Earth Surf. Processes Landforms **24**, 319 (1999).
[25] J.M.T. Stam, Sedimentology **44**, 127 (1997).
[26] An inapropriate boundary condition appears to be the main reason for the failure of the original attempts to model flow separation in this way [11].
[27] For most applications it is a matter of convenience how exactly the shear stress is set to zero inside the separation zone. For example, one may choose a form that mimics the theoretically expected [8] deposition of sand on the slip face without further adaptation of the model. In two dimensions one may also treat the brink as a boundary for the flux equation (see Sec. IV C).
[28] Fluent Inc., FLUENT5 (1999), finite volume solver.
[29] G. Sauermann, *Modelling of Wind Blown Sand and Desert Dunes* (Logos-Verlag, Berlin, 2001).
[30] P. Wesseling, *Principles of Computational Fluid Dynamics* (Springer, Berlin, 2000).
[31] G.F.S. Wiggs, I. Livingstone, and A. Warren, Geomorphology **17**, 29 (1996).
[32] R.S. Anderson, Acta Mech. (Suppl.) **1**, 21 (1991).
[33] P. Nalpanis, J.C.R. Hunt, and C.F. Barrett, J. Fluid Mech. **251**, 661 (1993).
[34] F. Rioual, A. Valance, and D. Bideau, Phys. Rev. E **62**, 2450 (2000).
[35] P.R. Owen, J. Fluid Mech. **20**, 225 (1964).
[36] J.P. Bouchaud, M.E. Cates, J. Ravi Prakash, and S.F. Edwards, J. Phys. I **4**, 1383 (1994).
[37] M.C. Malin *et al.*, Science **279**, 1681 (1998).
[38] P.C. Thomas *et al.*, Nature (London) **397**, 592 (1999).
[39] B. Andreotti and P. Claudin, e-print cond-mat/0201105.
[40] A.R. Lima, G. Sauermann, H.J. Herrmann, and K. Kroy, Physica A **310**, 487 (2002).